Supporting Information

Ma'ayan *et al*. 10.1073/pnas.0805344105

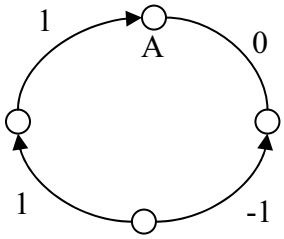

Fig. S1. Example of a 4-node-cycle with directed and undirected links.

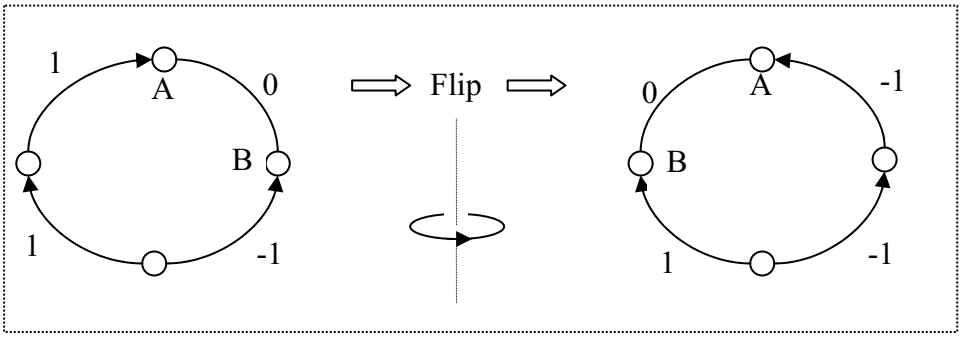

Fig. S2. A flip of the 4-node-cycle of Fig. 1 consists of turning the cycle over, while inverting the edge directions.

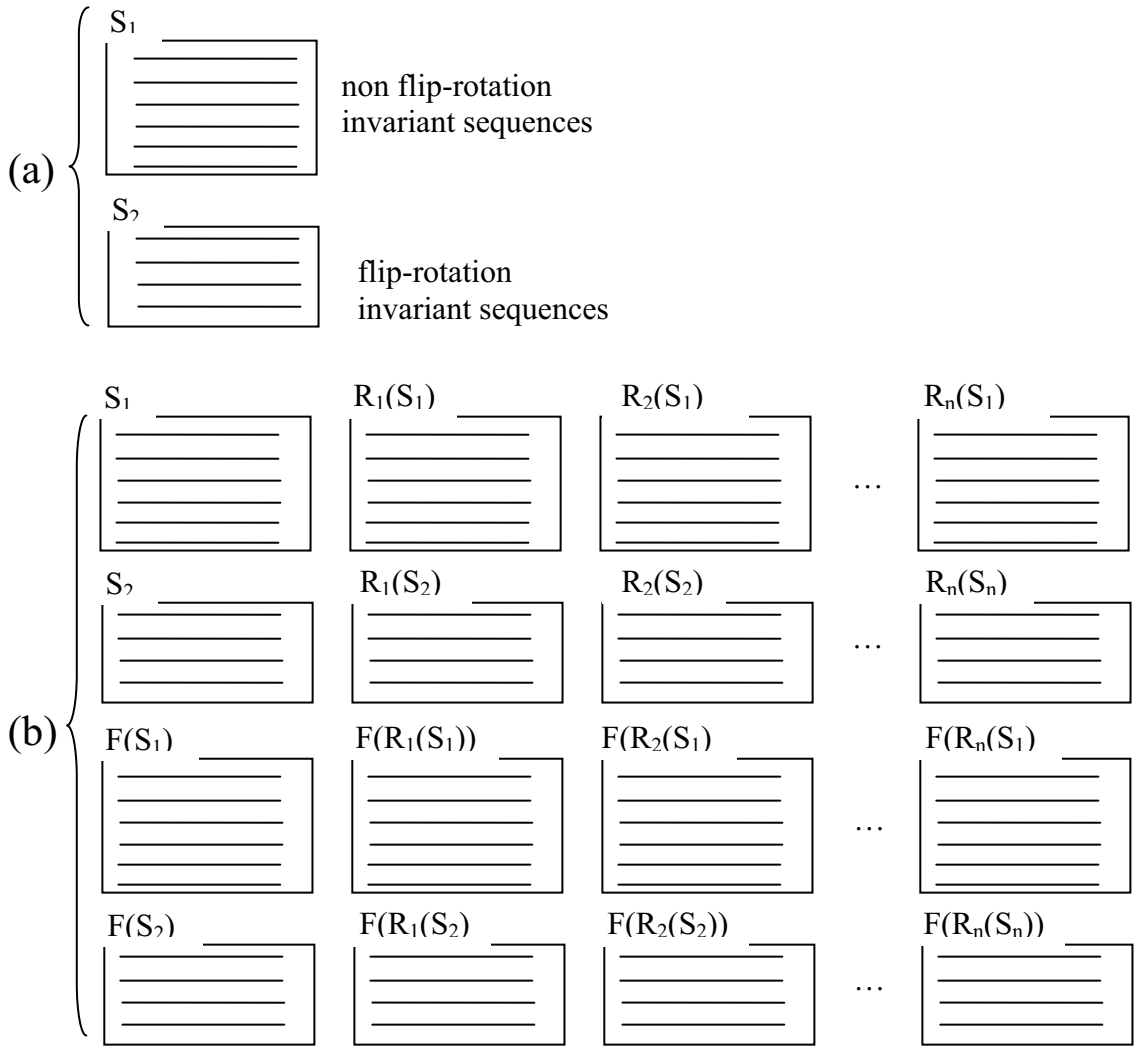

Fig. S3. Construction to count the number of unique directed cycles. (*a*) Assuming we know what those N_n cycles are, we divide them into the set S_1 of non-rotation-flip invariant and S_2 of rotation-flip invariant cycles. (*b*) For each sequence, we create all possible rotations, and flips, leading to a total of $2nN_n$ cycles.

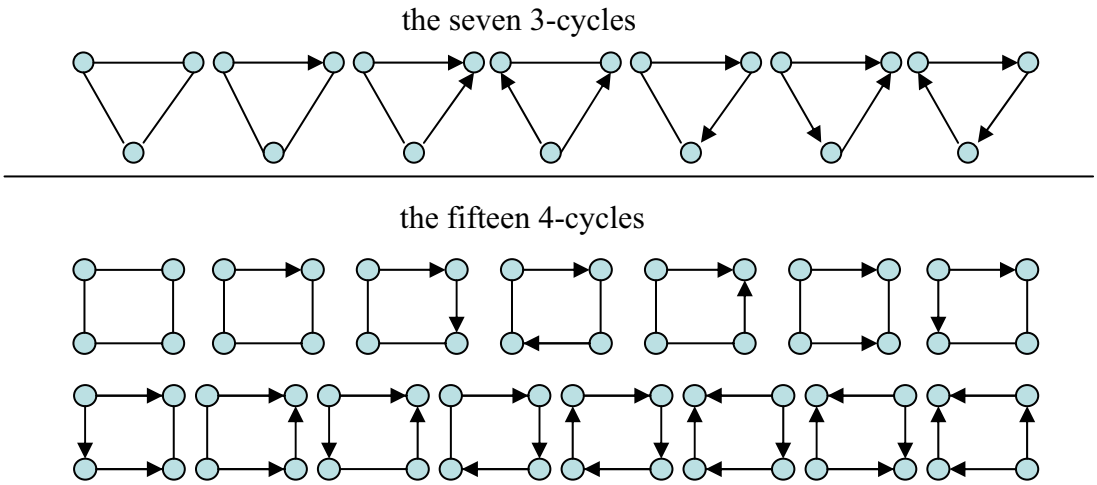

Fig. S4. The complete non-isomorphic list of 3- and 4-node-cycles.

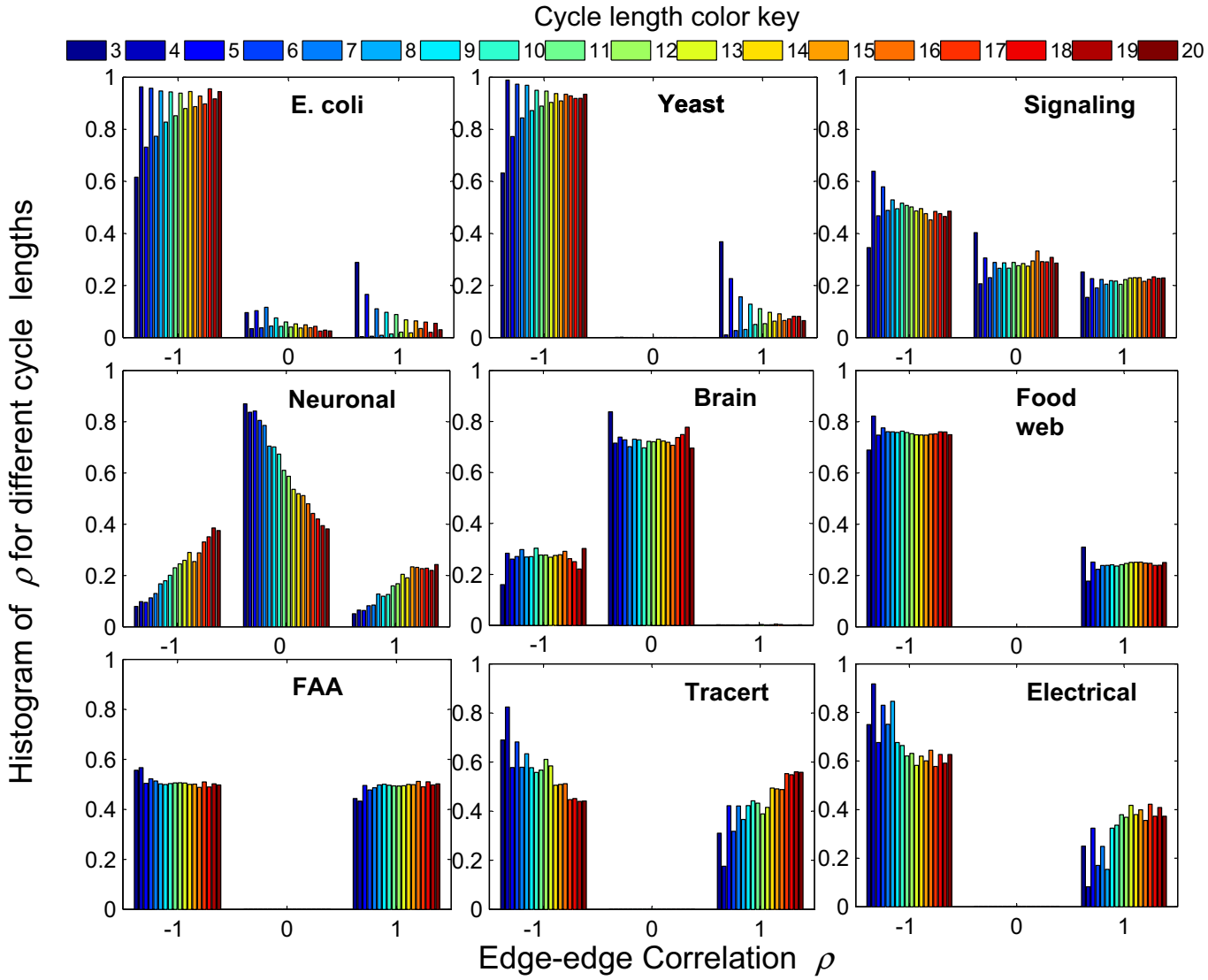

Fig. S5. Normalized histograms of the edge-edge correlation for the nine networks studied. $\rho = -1$, 0, and 1 correspond source/sink nodes, nodes with at least one neutral edge, and pass-through nodes. Each color corresponds to one cycle length, as indicated in the color key.

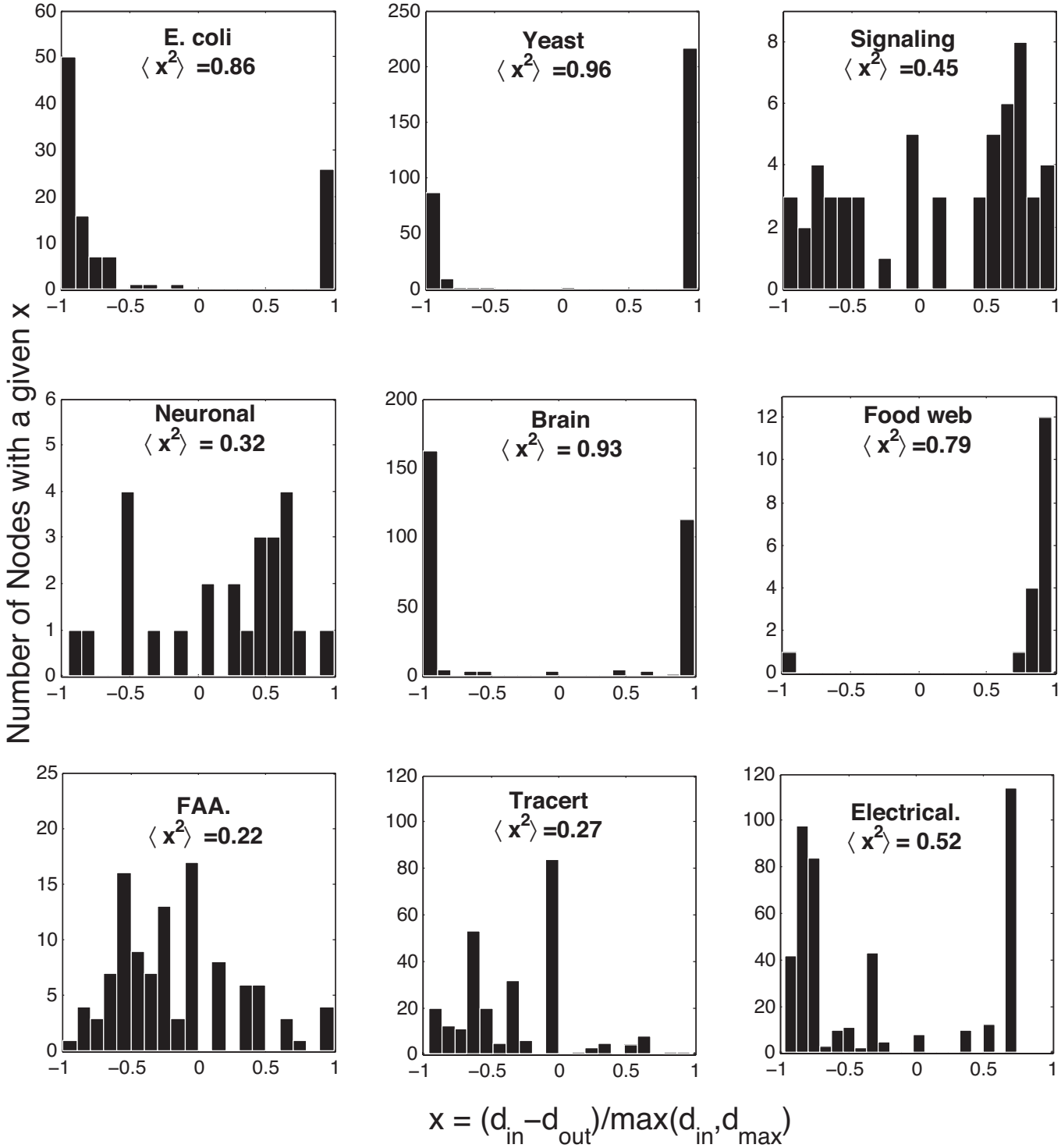

Fig. S6. The exclusion principle. If the postulated exclusion principle is operational, there would be a large number of nodes with exclusion principle measure close to $x = 1$ and/or $x = -1$. The figure shows that this is the case for some, but not all of the networks. The data correspond to nodes in the 10 upper percentile of the directed edge distribution (i.e., excluding neutral links).

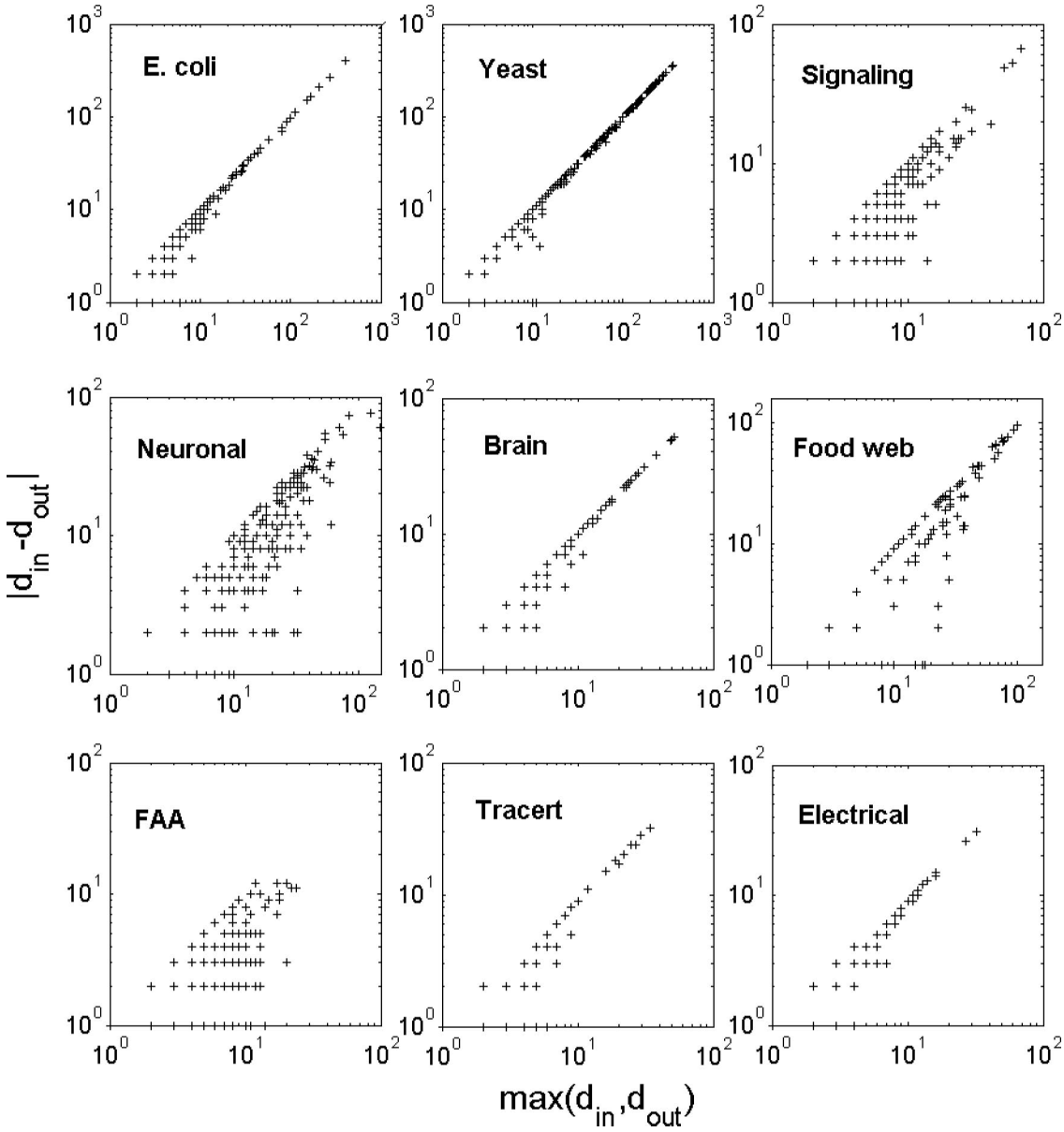

Fig. S7. A second view of the ''exclusion principle''. The horizontal axis is the maximum between the in- and out-degrees, and the vertical axis is the absolute value of the difference between the degrees, for each node. Each subpanel depicts the analysis for a different network.

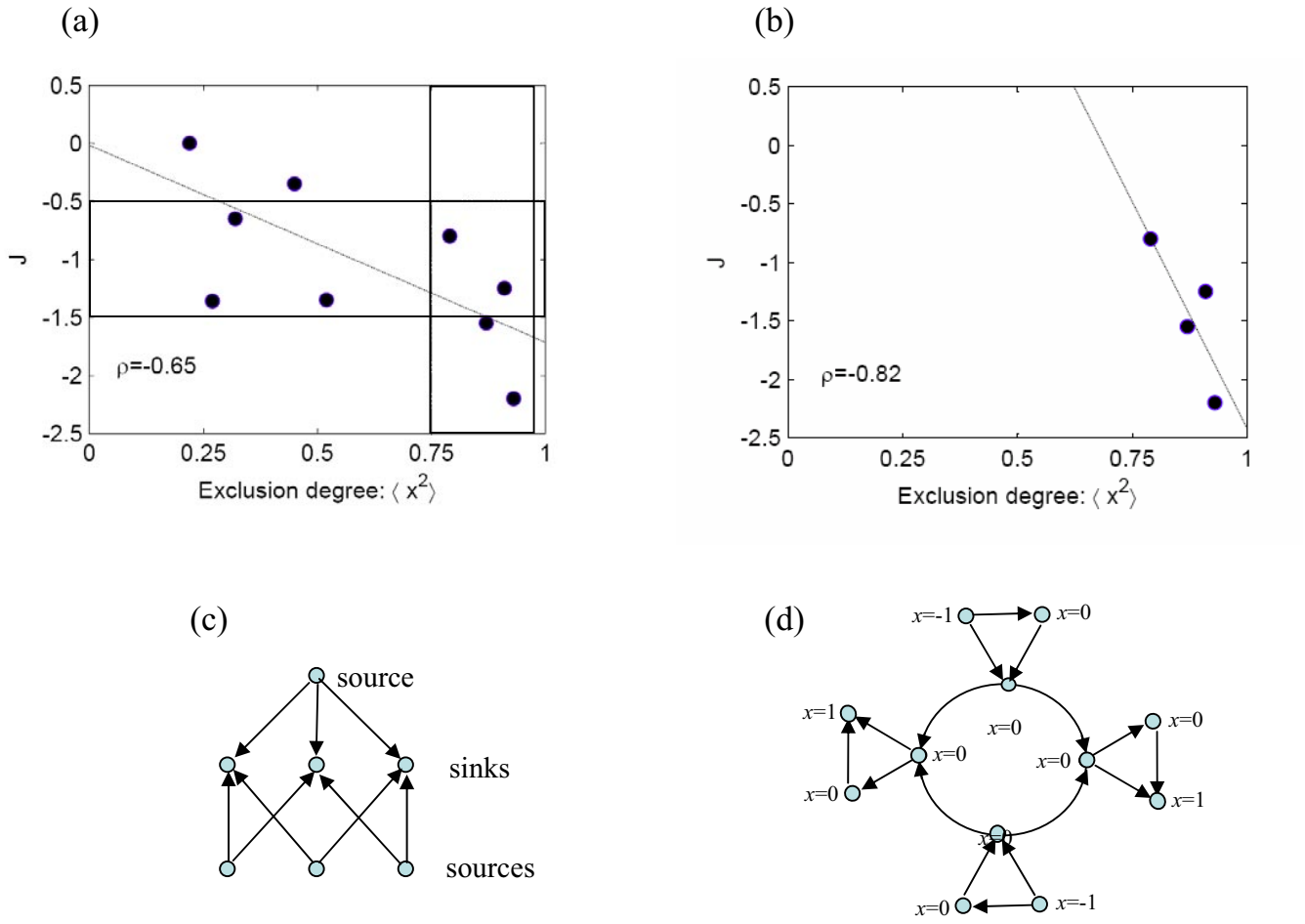

Fig. S8. The ''exclusion principle'' and antiferromagnetism. (*a*) there is a substantial correlation ($r = -0.74$) between the magnetic coupling J and the exclusion degree $\langle x^2 \rangle$. (*b*) The correlation is stronger ($r = -0.82$) in the region $\langle x^2 \rangle \gg 0.65$. The horizontal rectangle (*a*) contains points with antiferromagnetic J but weak exclusion degree. (*c*) Example where the exclusion principle leads to antiferromagnetism. (*d*) Examples where antiferromagnetism does not lead to exclusion principle.

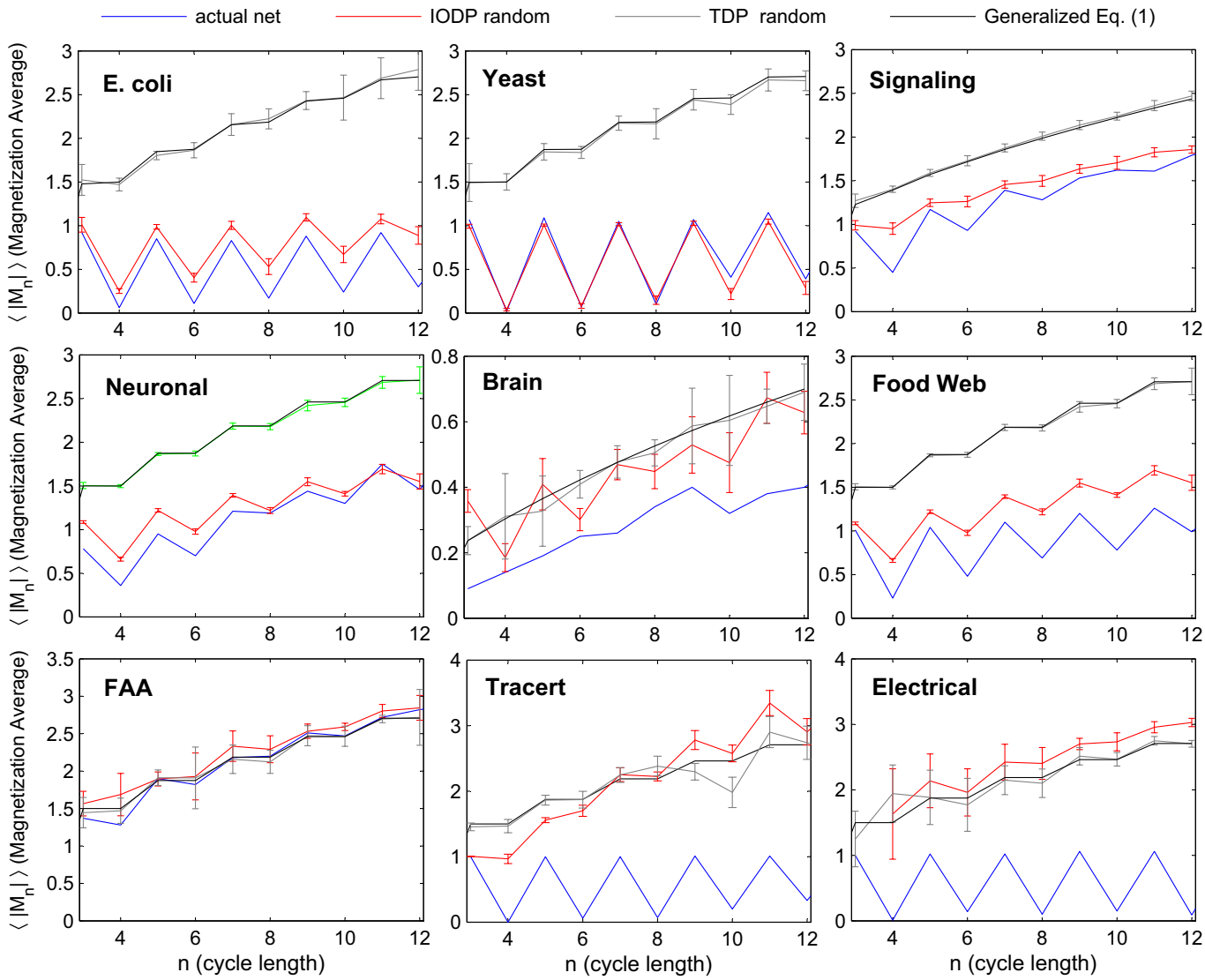

Fig. S9. Magnetization in real networks. The average of the absolute value of the magnetization for different cycle lengths in the indicated networks for the actual network (blue curves), the in-and out degree preserving (IODP) randomization (red curves), and the total-degree preserving (TDP) randomization. The black line corresponds to the theoretical expression derived in the *SI Appendix* for cycles with independent edges (a particular case of which is given in Eq. **1** of the main paper).

ecoli	z-score	brain	z	signaling	z	electr.	z	yeast	z	faa	z	foodweb	z	neuron	z
2252	28.049	990	5401.2	13214	43.571	204	876.02	206	50.093	2126	48.336	3038	145.54	46	6.626
718	26.534	9182	2811.2	13278	34.892	202	243.98	204	42.299	4958	47.371	2766	136.37	36	5.0978
462	18.228	734	2140.4	204	34.209	2182	229.4	2126	21.17	206	45.938	2182	122.12	238	5.0693
8910	15.696	17238	1682.5	990	27.25	2124	203.31	14	11.156	670	36.082	27342	97.678	78	-5.0512
398	14.439	862	946.3	17238	24.019	2076	163.93	2118	7.9355	2190	32.346	31710	95.794	14	-6.885
204	14.117	2462	943.93	17246	20.381	2118	130.62	2190	7.3285	2252	32.202	2270	93.899		
2188	13.155	4574	828.94	862	17.371	142	23.264	202	4.8908	734	31.987	18460	80.756		
2190	12.085	222	790.65	18636	14.858	392	5.0984	2252	4.4285	718	31.863	222	72.884		
206	11.377	4958	757.38	8732	14.816	652	3.0847	2076	4.2823	2140	31.809	18518	56.283		
710	11.246	18846	687.12	27340	14.267	2184	2.8858	2182	3.9872	204	30.923	2758	45.502		
142	8.8148	350	484.33	2758	13.687	140	2.7168	142	3.9388	462	29.094	2076	44.06		
604	8.3374	2782	426.3	4554	13.547	14	0.282	2188	3.4112	8606	28.048	14	42.735		
8908	7.2057	6558	258.3	19142	12.983	2188	0.0142	652	3.0151	142	27.783	2140	41.684		
334	5.9381	4510	251.41	350	12.009	536	-0.304	716	2.1566	2076	26.058	2252	34.054		
4494	4.9519	18518	224.41	16982	11.764	28	-7.1227	30	2.1329	5070	25.163	2202	25.812		
6302	4.3243	666	173.19	19148	11.744	74	-13.429	2124	1.1045	17302	24.787	392	25.448		
2124	4.2256	158	166.78	2182	11.185	2116	-19.372	2184	0.93481	4554	21.459	2254	24.345		
4574	4.0701	27030	134.87	14	10.592			590	0.84391	18634	21.343	18636	20.159		
716	4.0355	8908	121.45	9182	10.163			710	0.26384	2142	21.201	2184	18.633		
30	3.938	2398	106.48	19150	10.14			714	0.23853	2758	21.132	206	17.598		
14	3.4422	2458	106.29	8650	9.8458			536	0.1699	10398	21.018	204	16.739		

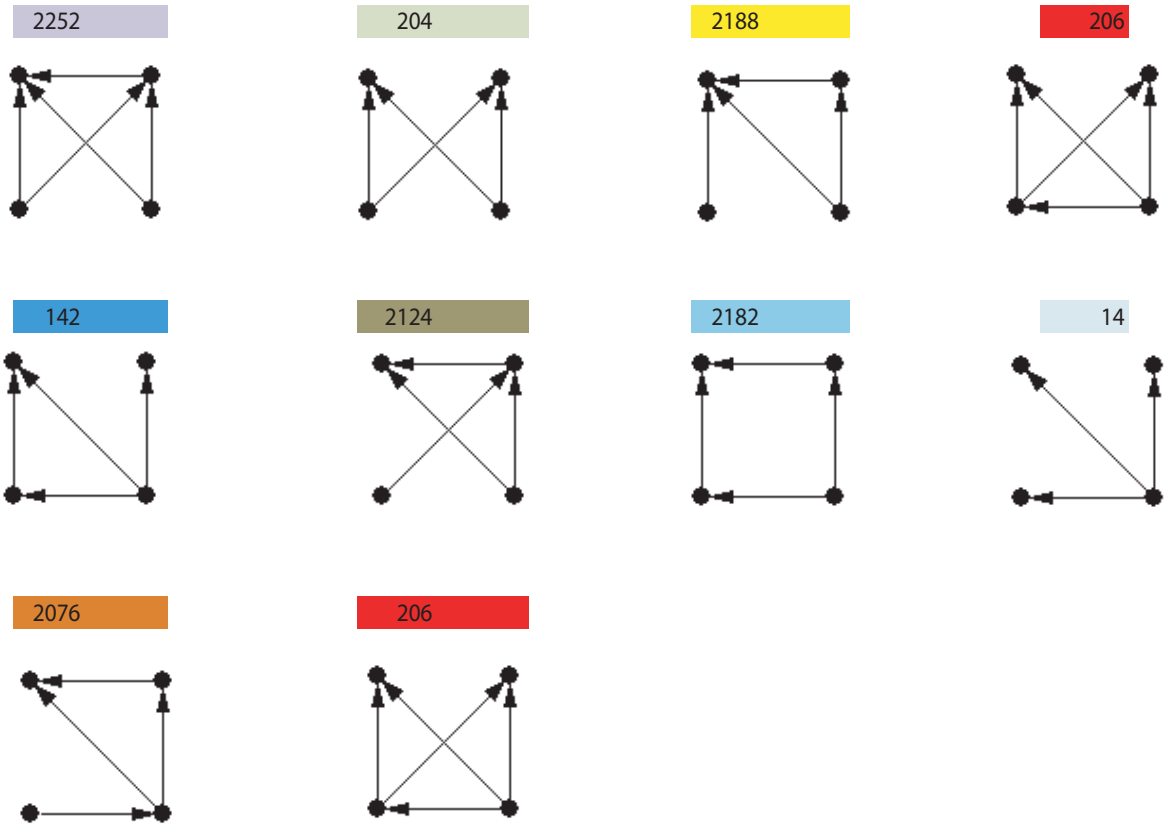

Fig. S10. Four-node network motifs identified using FANMOD. Motifs are listed for each network based on the *P* value of their significance. The motifs that are found in more than three networks are highlighted in different colors where the configuration is drawn below. The bifan motif has the motif ID 204. Note that bifans are also embedded in motifs 2252, and 206.

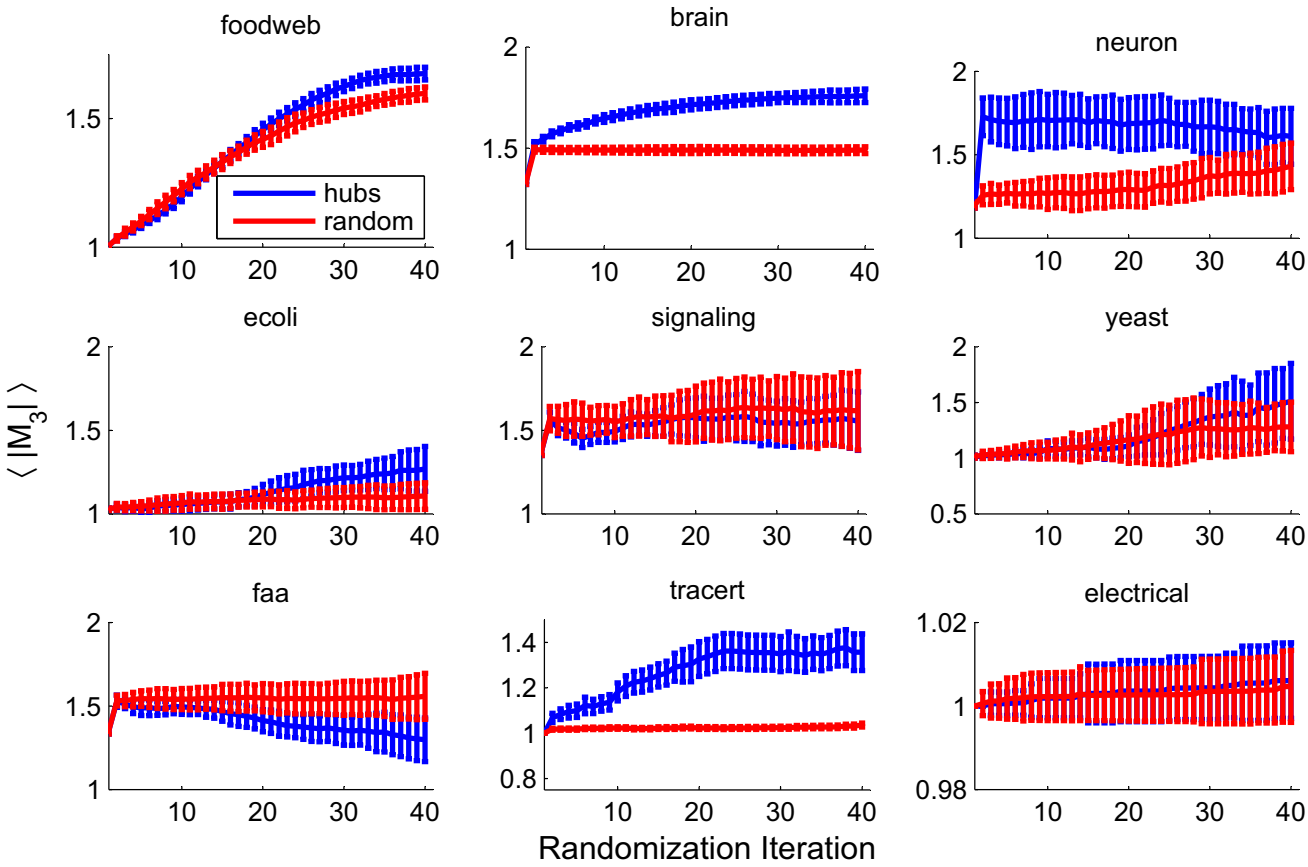

Fig. S11. In and Out degree hub removal and the magnetization of cycles of length $n = 3$. Surrogate networks generated by randomizing the links corresponding to the top out- and in-degree hubs (blue trace), and by randomizing the same number of links chosen from random nodes (red trace). In all cases, with the exception of the FAA network, the magnetization of cycles of size 3 increases with the randomization steps, as expected. In all cases (again, barring FAA), the hub-based surrogate shows higher or about the same magnetization as the random surrogate, consistent with our interpretation of a partial contribution of the hubs to antiferromagnetism.

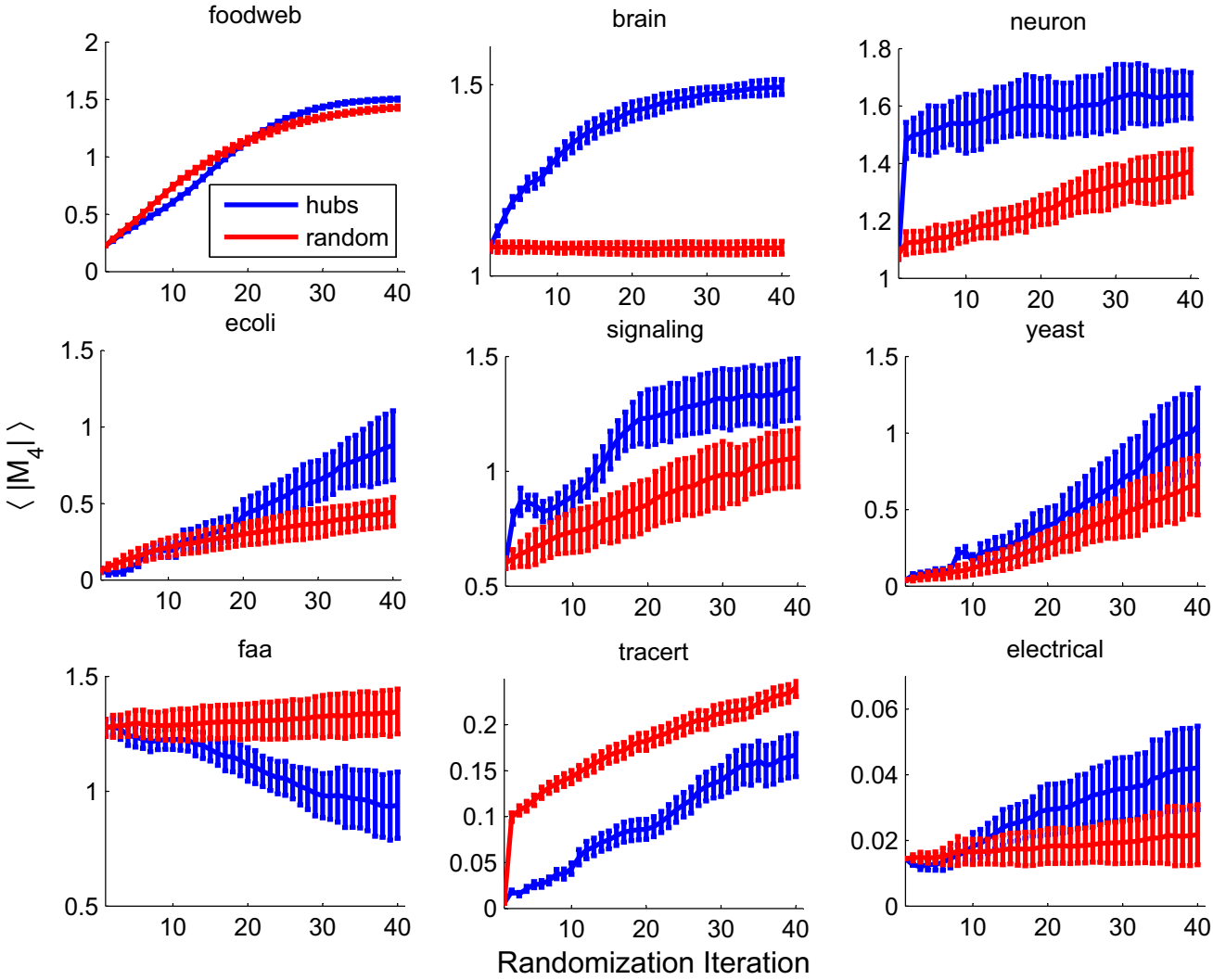

Fig. S12. In and Out degree hub removal and the magnetization of cycles of length $n = 4$. Same as in Fig. S11, for the magnetization of cycles of length 4.

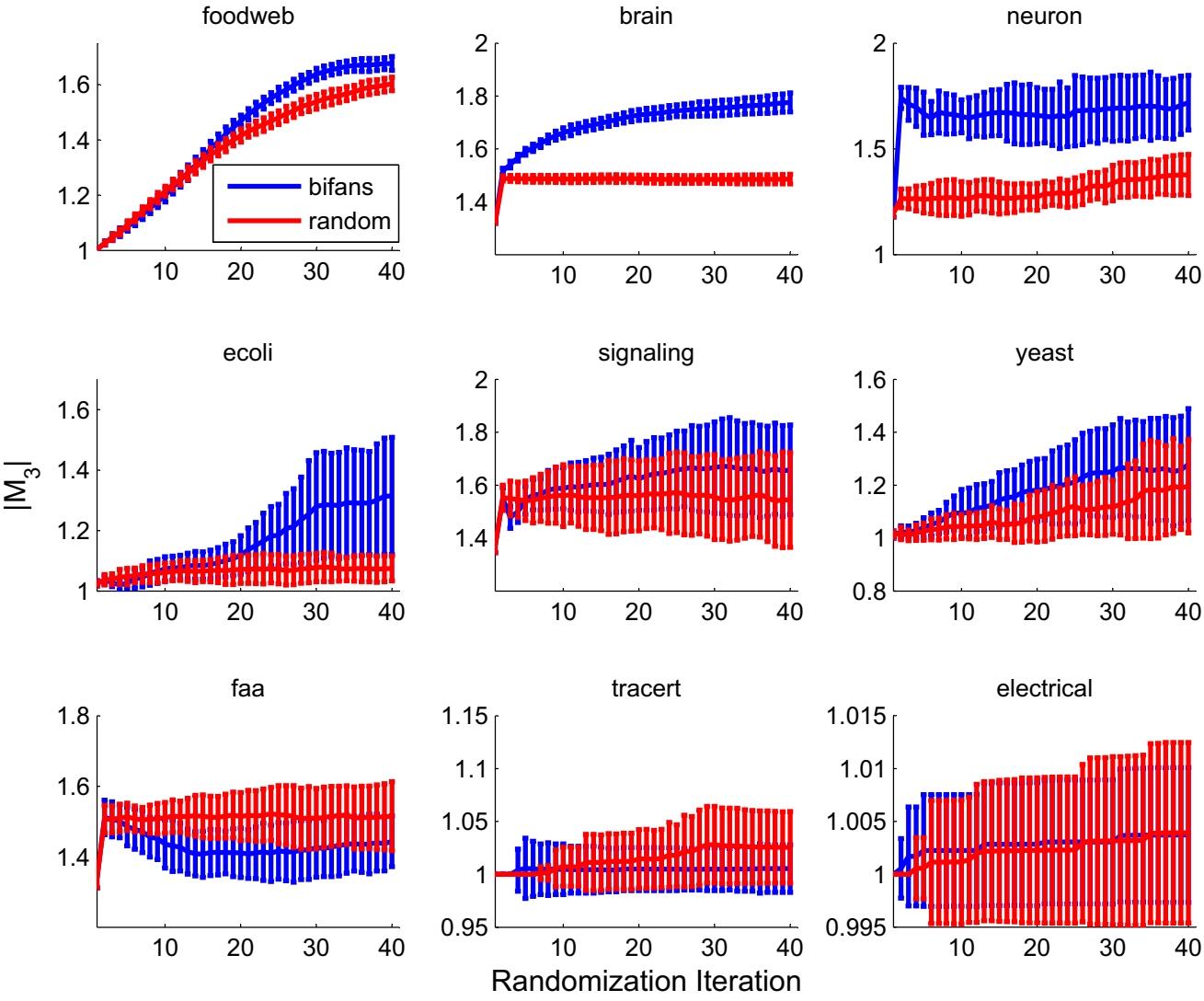

Fig. S13. Effect of bifan removal ($n = 3$). Surrogate networks generated by randomizing the links corresponding to the top out- and in-bifan hubs (blue trace), and by randomizing the same number of links chosen from random nodes (red trace). The effect is similar to what is observed for the degree hub removal, although the tracert and electrical networks do not show a significant trend for this cycle size.

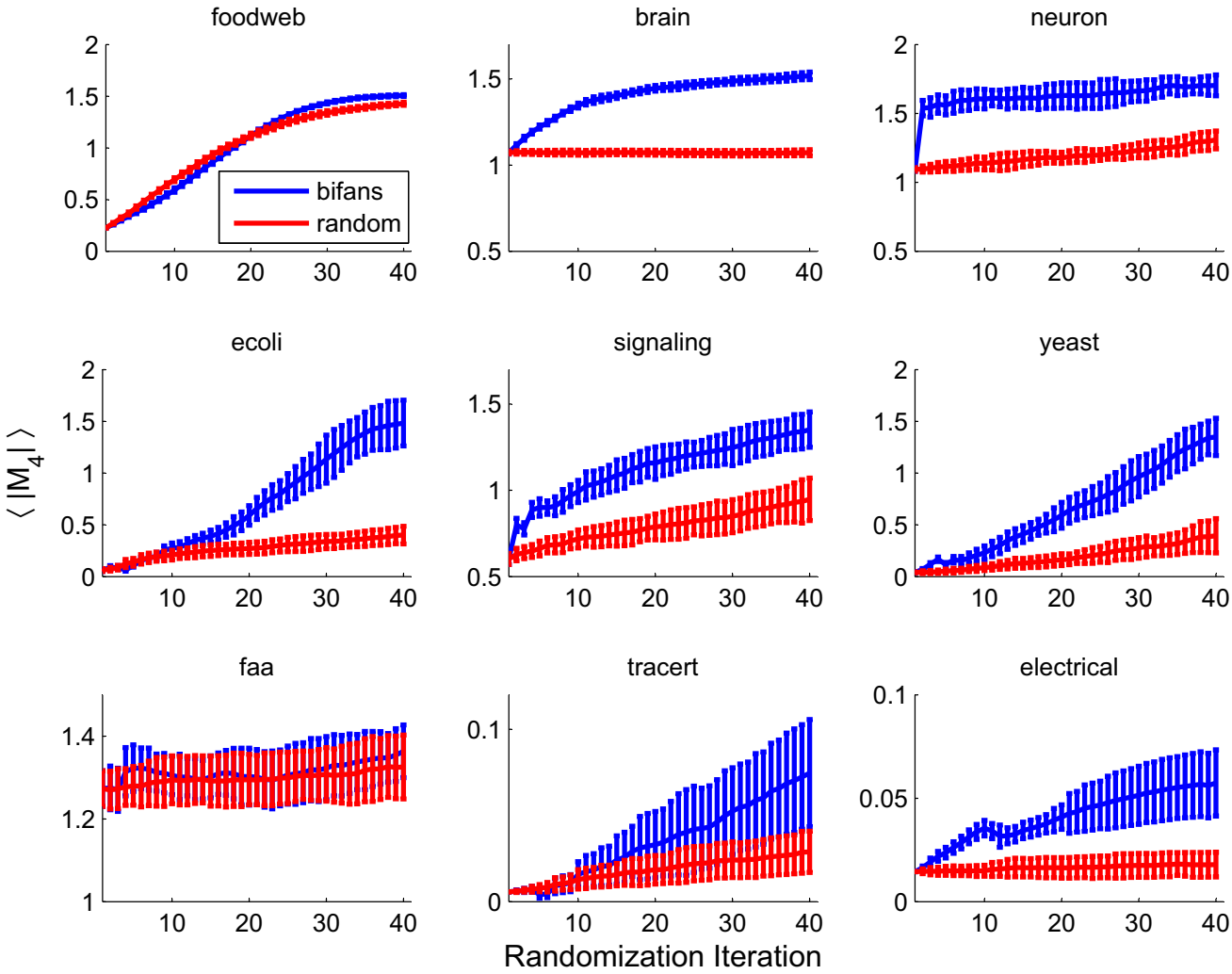

Fig. S14. In and Out bifan hub removal and the magnetization of cycles of length $n = 4$. Same as in Fig. S13, for cycles of length 4.

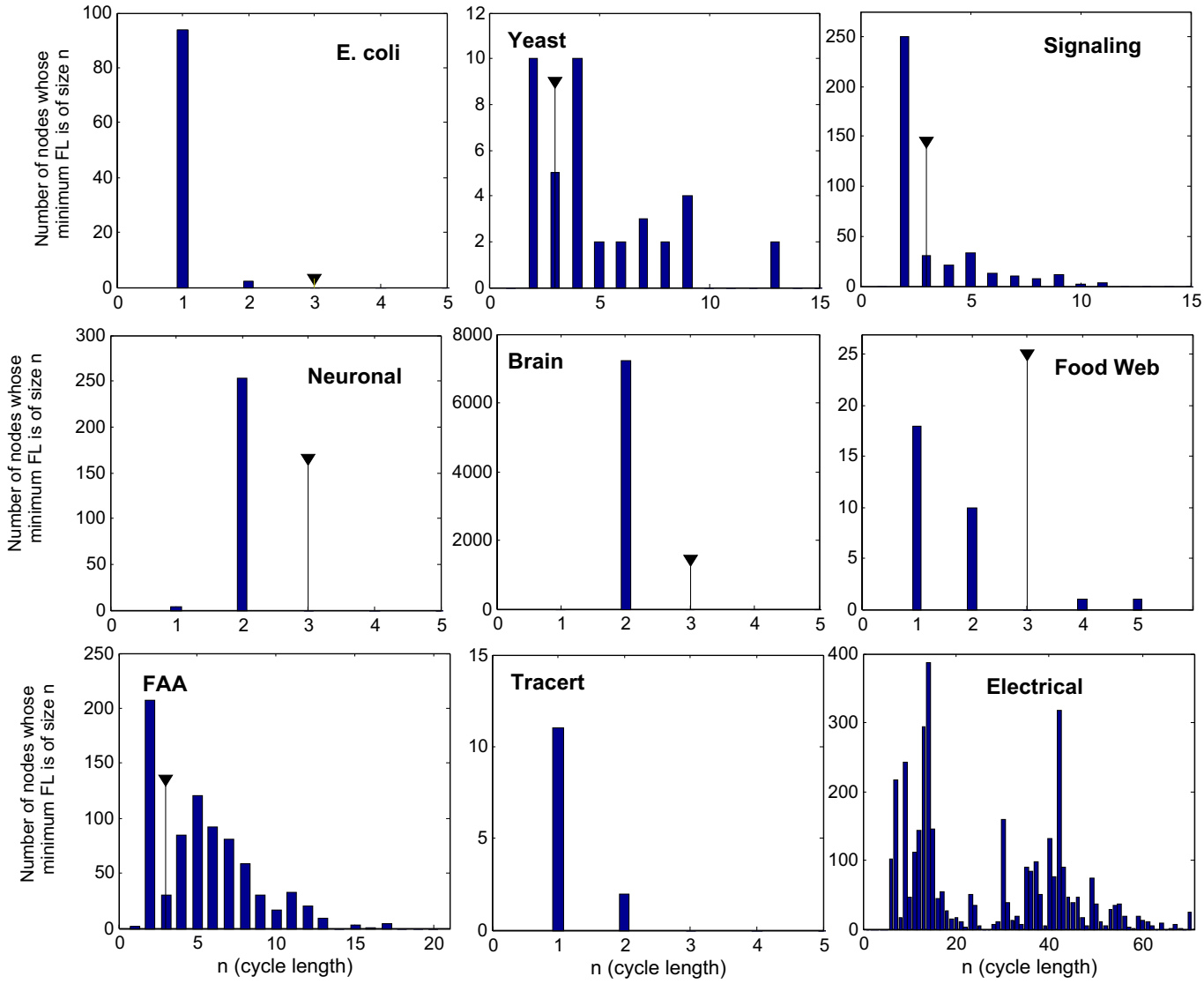

Fig. S15. Distribution of nodes that participate in at least one feedback loop, and whose minimum FL is of a given size. The plots show the number of nodes whose minimum feedback loop is of size n, for $n = 1, 2, \ldots$. The number of nodes with loops of length greater than 2 is underestimated. For example, the triangle-topped stem in each subfigure shows the actual number of nodes affected by feedback loops of size 3. The blue bars at $n = 3$ are shorter because some of the nodes participating in 3-loops were counted as participating in 2-loops and 1-loops.

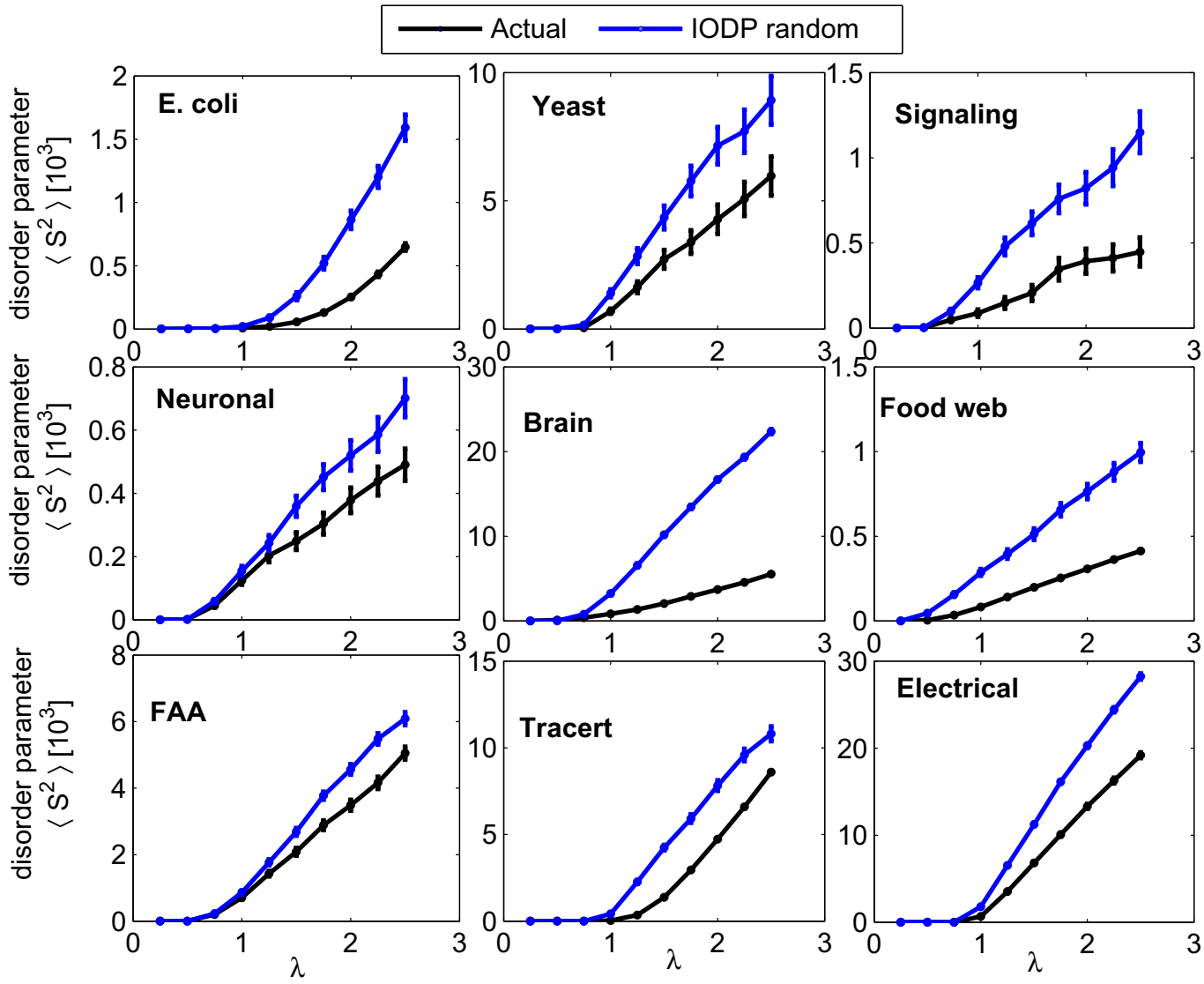

Fig. S16. Disorder parameter in all of the networks and their IODP randomizations. Each panel shows the disorder parameter $\langle S^2 \rangle$ (defined as the sum of the variances over all of the dynamic variables) for the actual network (black line) and the IOPD randomized surrogate (blue line) as a function the interaction strength between nodes, λ. The dynamics were simulated using Eq. **3** in the main text. Error bars in the plots correspond to the standard error in 100 simulations. It is clear that the actual networks exhibit a more ordered overall behavior compared with the IODP networks.

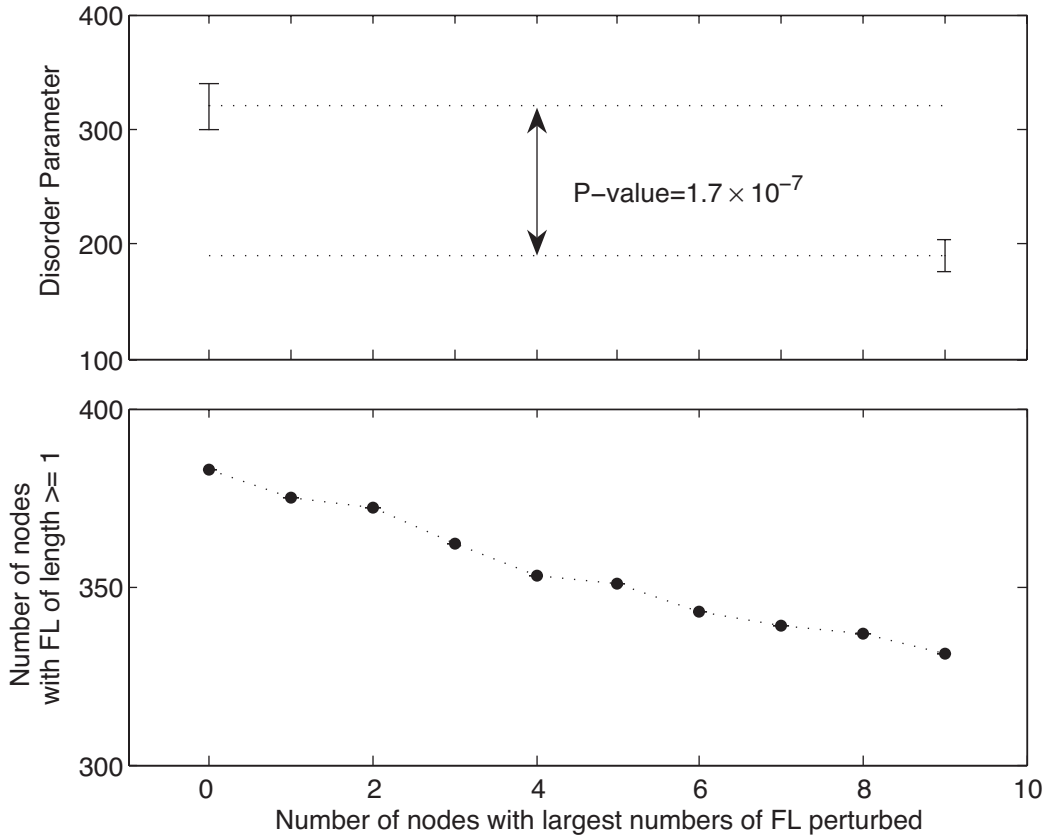

Fig. S17. The effects of node removal on the disorder parameter for the signaling network. We removed feedback loops by excising the links associated with the nodes affected with the most number of feedback loops (including 1-loops and 2-loops). We iterated this process for a total of 9 node removals. At the 0th removal and the 9th removal, we computed the disorder parameter. The network with fewer feedback loops had a significantly smaller disorder parameter.

Table S1. The rotation-flip invariant constraints for $k = 3$ and $n = 7$ for sequence s = s1 s2 s3 s4 s5 s6 s7

$R_3(s) = F(s)$
$s4 = \underline{s7}$
$s5 = \underline{s6}$
$s6 = \underline{s5}$
$s7 = \underline{s4}$
$s1 = \underline{s3}$
$s2 = \underline{s2} \rightarrow s2 = 0$
$s3 = \underline{s1}$

The underline in $\underline{sj}$ denotes $-sj$.

Table S2. The rotation-flip invariant constraints for $n = 6$ and $k = 3$ and 4, for sequence s = s1 s2 s3 s4 s5 s6

$R_3(s) = F(s)$	$R_4(s) = F(s)$
$s4 = \underline{s6}$	$s5 = \underline{s6}$
$s5 = \underline{s5} \rightarrow s5 = 0$	$s6 = \underline{s5}$
$s6 = \underline{s4}$	$s1 = \underline{s4}$
$s1 = \underline{s3}$	$s2 = \underline{s3}$
$s2 = \underline{s2} \rightarrow s2 = 0$	$s3 = \underline{s2}$
$s3 = \underline{s1}$	$s4 = \underline{s1}$

The underline in $\underline{sj}$ denotes $-sj$.

Table S3. The rotation-flip invariant constraints for $k = 2$ and $n = 4$ for sequence s = s1 s2 s3 s4

$R_2(s) = F(s)$
$s3 = \underline{s4}$
$s4 = \underline{s3}$
$s1 = \underline{s2}$
$s2 = \underline{s1}$

The underline in $\underline{sj}$ denotes $-sj$.

Table S4. The rotation-flip invariant sequences for $k = 2$ and $n = 4$

	X	$\underline{X}$	Y	$\underline{Y}$		X	$\underline{X}$	Y	$\underline{Y}$
A	−1	1	−1	1	D	1	−1	0	0
B	0	0	−1	1	R_2(C)	−1	1	1	−1
C	1	−1	−1	1	R_2(D)	0	0	1	−1
R_2(B)	−1	1	0	0	R_1(A)	1	−1	1	−1
Z	0	0	0	0					

Except for the all-zero sequence, for each of these sequences there is a different but rotation-equivalent one in the set.

Table S5. All the sequences of period *p* equal to 1, 2, and (a subset of) 4, that have a period that start at the beginning of the sequence and one (possibly the same) that end at location *j*

S					$R_1(s)$					$R_2(s)$					$R_3(s)$				
0	0	0	0	[1,1]	0	0	0	0	[2,2]	0	0	0	0	[3,1]	0	0	0	0	[4,1]
−1	−1	−1	−1	[1,1]	−1	−1	−1	−1	[2,2]	−1	−1	−1	−1	[3,1]	1	−1	−1	−1	[4,1]
1	1	1	1	[1,1]	1	1	1	1	[2,2]	1	1	1	1	[3,1]	1	1	1	1	[4,1]
0	−1	0	−1	[2,2]	−1	0	−1	0	[2,2]	0	−1	0	−1	[4,2]	−1	0	−1	0	[4,2]
0	1	0	1	[2,2]	1	0	1	0	[2,2]	0	1	0	1	[4,2]	1	0	1	0	[4,2]
1	−1	1	−1	[2,2]	−1	1	−1	1	[2,2]	1	−1	1	−1	[4,2]	−1	1	−1	1	[4,2]

These sequences are indicated with the annotation of [*p*,*j*].

Table S6. The number of classes of the first 15 *n*-node-cycles

n	N_n
3	7
4	15
5	30
6	74
7	171
8	444
9	1138
10	3048
11	8175
12	22427
13	61686
14	171630
15	479411

Table S7. Size of the networks analyzed in this study

Network	Nodes	Number of links: directional + 2 × non/bidirectional
E. coli	1,444	3,354
Yeast	4,084	9,997
Signaling	599	1,706
Neuronal	283	1,469
Foodweb	183	2,494
Brain	7,227	21,014
Electrical	5,844	8,199
FAA	1,226	2,615
Tracert	3,094	3,073

For the total number of links, the symmetric links are counted twice (i.e., the *ij* and the *ji* directions are counted), even though for some of the networks some of these edges may represent nondirectional links.

Table S8. Counts of self-loops and feedback loops between pairs of nodes

Network	Self-loops	Two-node loops
Yeast	0	5
E. coli	94	8
Signaling	0	307
Foodweb	18	42
Neuronal	3	606
Brain	0	10,036
Electrical	0	0
Tracert	11	1
FAA	2	205

In the count for the total number of two-node loops, all the symmetric links are counted even though for some of the networks some of these edges may represent nondirectional links.

Other Supporting Information Files

Appendix (PDF)